Multimodal Imaging observation of Bietti crystalline dystrophy progression

Shengjuan Zhang

1. Beijing Institute of Ophthalmology, Beijing Ophthalmolgy and Visual Science Key Laboratory, Beijing Tongren Eye Center, Beijing Tongren Hospital, Capital Medical University. 2. Hebei Provincial Key Laboratory of Ophthalmology, Hebei Provincial Eye Institute, Hebei Provincial Eye Hospital.
https://orcid.org/0000-0003-4988-0953

Qian Li

Beijing Institute of Ophthalmology, Beijing OPhthalmolgy and Visual Science Key Laboratory, Beijing Tongren Eye Center, Beijing Tongren Hospital, Capital Medical University

Lifei Wang

Hebei Provincial Key Laboratory of Ophthalmology, Hebei Provincial Eye Institute, Hebei Provincial Eye Hospital

XiaoYan Peng (74000041@ccmu.edu.cn)

Hebei Provincial Key Laboratory of Ophthalmology, Hebei Provincial Eye Institute, Hebei Provincial Eye Hospital https://orcid.org/0000-0002-3946-5724

Research article

Keywords: Bietti crystalline dystrophy, Fundus autofluorescence, Infrared autofluorescence, Fundus fluorescein angiography, Spectral domain optical coherence tomography

Posted Date: December 7th, 2020

DOI: https://doi.org/10.21203/rs.3.rs-121910/v1

Abstract

Background

Bietti crystalline dystrophy (BCD) is an autosomal recessive genetic disorder that causes progressive vision loss in patients. Here, we observed the imaging characteristics of BCD development using a multimodal imaging model.

Methods

Color fundus photography, fundus autofluorescence (FAF), infrared autofluorescence (IRAF), fundus fluorescein angiography (FFA), and spectral domain optical coherence tomography (SD-OCT) were used for observation of 8 eyes of 4 patients (P1-P4) with BCD.

Results

Color fundus photography showed a decrease in the number of crystalline deposits in all 8 eyes. P1 and P2 showed expanded lesion and hypo-AF areas, and IRAF images revealed choroid macrovascularitis in the hypo-IRAF region. P1's lesion edge showed hyper-AF and (fewer) hyper-IRAF spots. P2's lesion edge showed hyper-AF but no hyper-IRAF spots. P3 and P4 showed patchy hypo-AF areas that were enlarged and partially merged together, as well as small numbers of hyper-AF spots, but no hyper-IRAF spots. FFA showed enlargement of the lesion area. P1 and P2 showed expanded hypo-fluorescence in the posterior pole. A mottled fluorescence around the hypo-fluorescence and at the periphery, expanding to the middle periphery. P3 both eyes contained a large hypo-fluorescence area around macular area and in the middle peripheral area, with mottled fluorescence in the macular area and the peripheral area. P4 showed slight residual mottled fluorescence, whereas the entire fundus showed a large area of choroid macrovascular fluorescence. P3 and P4 showed a significant reduction in the retinal mottled fluorescence area and more clearer choroid macrovascular fluorescence, similar to the early Indocyanine green angiography (ICGA) images. Optical coherence tomography (OCT) revealed retinal and choroidal thinning, progressive loss of the outer nuclear layer and ellipsoid zone (EZ), and shortening of the choroid macrovascular diameter.

Conclusions

BCD disease develops rapidly and can progress significantly in a short time in some cases. FAF, IRAF, and OCT are advantageous non-invasive models for detecting and assessing this disease.

Background

Bietti crystalline dystrophy (BCD) is an autosomal recessive genetic disorder first reported by Dr. Bietti in 1937 [1]. BCD causes progressive vision loss in patients due to mutations in the CYP4V2 gene that

encodes the CYP4V2 protein and is relatively common among Asian people, and especially among Chinese and Japanese persons, but it is rare among European and American people [2, 3]. BCD is characterized by the accrual of large amounts of yellowish crystals deposits at the posterior pole of the retina, retinal pigment epithelium (RPE) atrophy, and choroid sclerosis [4]. BCD has been receiving more attention in recent years, and reports on BCD have increased. However, most articles have focused on gene diagnosis [5, 6], cross-sectional imaging studies [7, 8], and case reports [9, 10]. Few studies have conducted follow-up observations, and most of these are case reports [11, 12].

Our aim in the present study was to use color fundus photography, fundus autofluorescence (FAF), infrared autofluorescence (IRAF), fundus fluorescein angiography (FFA), and spectral domain optical coherence tomography (SD-OCT) to observe the progression of retinal and choroidal changes in 8 eyes of 4 patients with BCD. Our overall goal was to gain a better understanding of BCD progression and changes.

Methods

Subjects

The implementation of all research methods in this study followed the provisions of the Declaration of Helsinki, the Ethics Committee of Beijing Tongren Hospital, Capital Medical University, and the Ethics Committee of Hebei Provincial Eye Hospital. This study included 4 unrelated Chinese patients who visited our hospital twice between January 2017 and October 2018 and were diagnosed with BCD after clinical examination. The clinical characteristics and imaging data of these patients were retrospectively analyzed. For convenience, cases 1, 2, 3, and 4 included in this study are referred to as P1, P2, P3, and P4 respectively. The intervals of P1, P2, P3, and P4 were 10, 16, 20, and 20 months respectively. According to the staging criteria proposed by Yuzawa et al [13], the stage of the fundus lesions at the first visit to our hospital were as follows: P1 and P2 were stage 2, with RPE atrophy extending to the mid-peripheral area, with choroidal capillary atrophy. P3 and P4 were stage 3, with extensive RPE and choroidal capillary atrophy. The first examination of the 4 patients was referred to as P1F, P2F, P3F, and P4F, and the last examination was referred to as P1L, P2L, P3L, and P4L.

All 4 patients included in this study agreed to undergo a genetic diagnosis at our hospital. Peripheral venous blood was collected upon receiving signed informed consent. The genomic DNA was extracted from the blood and the BCD pathogenic gene CYP4V2 was sequenced. Further sequence alignments and mutation screenings were also performed.

Procedures

All patients underwent complete ophthalmic examinations, including best corrected ETDRS visual acuity (BCVA), slit-lamp microscopy, Goldman tonometry, indirect dilatation fundus examination, and fundus photography (Kowa, Nonmyd 7, Kowa, Japan).

The FAF, IRAF, and FFA images over a 55×55° field were obtained with a confocal scanning laser ophthalmoscope (Heidelberg Spectralis, Heidelberg Engineering, Heidelberg, Germany). The results of the two examinations were compared and changes were documented.

SD-OCT images were adopted by a Spectralis Optical coherence tomography (OCT) (Heidelberg Engineering, Heidelberg, Germany). The Spectralis SD-OCT scanning mode for horizontal linear scans selects and enhances the depth imaging (EDI) mode. Each scan was centered on the macular fovea (because the fovea OCT images of the P1 left eye and P2 left eye were not scanned during the first examination, and the scanning image was slightly deviated from fovea. In the last examination, we followed the scans to track changes at this slightly deviated level. For convenience, in this study, the lowest point of the fovea shown at this level is also described as a fovea). Measurement data included the central macular thickness (CMT) and subfoveal choroidal thickness (SCT) [14]. The measurements were made on choroidal macrovascularities selected from the nasal side and the temporal side of the subfoveal choroid. The diameter of the vessel was measured to calculate the difference in blood vessel diameter between the first and the last examination and the changes were recorded. The ellipsoid zone (EZ) at the fovea of the P1 right eye is missing, but the residual EZ was seen at the temporal side of the fovea. The distance between the residual EZ at the proximal foveal end and the Bruch membrane below the fovea was measured and the difference calculated between the first and the last measurements. Little residual EZ was seen at the central fovea of the P1 left eye, the P2 and P4 both eyes. The EZ width was used to calculate the difference between the first and the last measurements; the EZ of P3 both eyes macular area is missing.

Results

The general conditions and genetic diagnosis results for P1-P4 are shown in Table 1 and Table 2.

The mean patient age was 34.75 ± 5.75 years. The BCVA (ETDRS) of the 8 eyes was significantly decreased, with a mean decrease of 14.5±17.5.

Fundus photography

The yellowish crystalline deposits in the posterior pole of the retina were reduced at the last examination. A greater atrophy of the retinal pigment epithelium (RPE) choriocapillaris complex was associated with fewer yellowish crystals. The numbers of pigmentation plaques scattered in the posterior retina increased (Fig. 1C), and part of the original pigment plaque was larger at the last examination (Fig. 1D).

Fundus autofluorescence (FAF) and infrared autofluorescence (IRAF)

The lesions area shown by FAF and IRAF were consistent in the P1 and P2 both eyes. Significant expansion of the hypo-AF and hypo-IRAF area at the macular area and around optic papilla area was observed, and the partial patchy hypo-AF areas merged together. IRAF revealed the choroid macrovascular morphology in the posterior hypo-IRAF area. The hypo-IRAF area was larger than the hypo-

AF area. In P1, the hyper-AF spots and hyper-IRAF spots were observed at the junction of the hypo-AF and normal retina and the hypo-IRAF and normal retina. The number of hyper-AF spots was significantly greater than the number of hyper-IRAF spots. Because the lesion area was extended, this changed the position of the hyper-AF spots and hyper-IRAF spots compared with P1F, but the quantity of spots showed no obvious change. Comparison of P2L and P2F revealed a reduction in the number of hyper-AF spots. No obvious hyper-IRAF was found in P2F or P2L (Fig. 2A-H).

Comparison of P3L versus P3F and of P4L versus P4F revealed significant expansion of the hypo-AF area at the macular area and around the optic papilla area, with partial patchy hypo-AF merged together. IRAF showed the hypo-IRAF morphology of optic disc, retinal macrovascularities, and choroidal macrovascularities. P3 and P4 showed hyper-AF spots, but no hyper-IRAF spots. P3 and P4 also showed uneven autofluorescence intensity of the hypo-AF areas, but the corresponding IRAF spots showed uniform hypo-IRAF, revealing hypo-IRAF of the choroidal macrovascularities (Fig. 2I-P).

Fundus fluorescein angiography (FFA)

The posterior region of the P1F both eyes showed choroidal macrovascular fluorescence in hypo-fluorescence area, with surrounding mottled fluorescence. The peripheral retina showed mottled fluorescence. Annular normal retinal fluorescence was seen in the mid-peripheral area. The lesions of the posterior and peripheral parts of the P1L both eyes extended to the mid-peripheral parts, and the atrophic hypo-fluorescence of the RPE choriocapillaris complex in the posterior and superior peripheral parts was larger than that of P1F (Fig. 3A-D).

In the macular area and around the optic papilla area of the P2F both eyes, choroidal macrovascular fluorescence was observed in hypo-fluorescence area, with surrounding mottled fluorescence. Partial normal retinal fluorescence was evident between the temporal peripheral lesion area and the macular lesion area. The hypo-fluorescence area in the posterior of the P2L both eyes was enlarged, the mottled fluorescence was more disordered than in P2F, and the normal retinal fluorescence of the macular area temporal side was reduced because of the progression of the surrounding lesions (Fig. 3E-H).

The posterior patchy hypo-fluorescence areas of the P3F both eyes reached the mid-peripheral area and the rest of the retina outside the hypo-fluorescence area, including part of the macular area, which showed mottled fluorescence. The posterior patchy hypo-fluorescence was enlarged and partially merged together. The hypo-fluorescence was mainly expanded to the periphery, and no obvious changes were noted in the mottled fluorescence in macular area (Fig. 3I-L).

In addition to the mottled fluorescence of the superior temporal, temporal, and inferior peripheral retina, choroidal macrovascular fluorescence was observed in other regions of the P4F both eyes. The mottled fluorescence of the superior temporal, temporal, and inferior peripheral retina was smaller in P4L than in P4F, and the choroidal macrovascular fluorescence in the other area was clearer than in P4F (Fig. 3M-P).

Spectral domain optical coherence tomography (SD-OCT)

The outer nuclear layer, EZ, interdigitation zone, and RPE in the macular area of P1-P4 showed atrophy to different degrees, and a partial reflection was missing. The outer retinal tubulation (ORT) could be seen in some layers. OCT-related data from the P1-P4 first and last examinations were recorded. Retinal thickness in the fovea was thinner in all eyes except the P1 left eye and P3 left eye, with an average thickness of 24.428±48.572 μm. The macular edema of the P1L left eye was increased over that of P1F, so the CMT was increased by 12 microns. The CMT of the P3 left eye showed no obvious change. The SCT of all 8 eyes were thinner, with an average thickness of 42.125±50.875 μm. The diameter of the temporal side choroidal macrovascular was reduced in all 8 eyes by an average of 21.125±18.875 μm. The diameter of the P1, P2, and P4 nasal side choroidal macrovascularities were reduced by an average of 22.5±15.5 μm. The diameter of the P3 nasal side choroidal macrovascular showed no obvious change; The residual EZ length of the P1 left eye, P2 both eyes, and P4 both eyes was shortened by an average of 269.4±206.6μm. No residual EZ was detected in the fovea of the P1 right eye, so we measured the distance between the temporal residual EZ proximal foveal end and the Bruch membrane below the fovea, the difference between P1F and P1L was 165 μm. The EZ and interdigitation zone were absent in the P3 both eyes macular area. The residual EZ only existed at the fovea of P2 and P4 and was absent at the nasal and temporal fovea. P1F had a small number of intraretinal cystoid cavities in the inner nuclear layer of the right eye and no intraretinal cystoid cavities in the left eye. The number of intraretinal cystoid cavities in the inner nuclear layer of the right eye was greater in P1L than in P1F, inner nuclear layer intraretinal cystoid cavities were present in the left eye of P1L, and the outer nuclear layer was thicker in P1L than in P1F. No intraretinal cystoid cavities were found in the macular area in the two examinations of P2 and P3. No intraretinal cystoid cavities were detected in the macular area of P4F but they were detected in countable numbers in P4L. (Fig. 4A-P).

Discussion

Our examination of multimodal images of 8 eyes of 4 BCD patients (P1, P2, P3, and P4) at different time intervals of 10, 16, 20, and 20 months, respectively, revealed expansion of the areas of hypo-AF and hypo-IRAF but a decrease in the hyper-AF spots and hyper-IRAF spots. FFA showed that the lesion area expanded and the hypo-fluorescence area with severe atrophy also expanded. OCT showed thinning of both the retina and choroid and progressive atrophy of the outer nuclear layer, EZ, and RPE, as well as significant thinning of diameter of the choroidal macrovascularities.

The four patients ranged in age from 29 to 38 years, which is the common onset age of BCD [15, 16]. The results of gene examinations were all showed BCD-related gene alleles [17, 18]. The BCVA (ETDRS) of all 8 eyes significantly decreased. Color fundus photography showed yellowish crystalline deposits in the posterior fundus. The number of yellowish crystalline deposits declined by the last examination, which was consistent with previous studies [12, 15, 19, 20]. The deposition of yellowish crystalline lipids is caused by abnormal expression of the CYP4V2 gene in the human retina and RPE [16, 21, 22], and it is reduced with atrophy of the retina and RPE.

Comparison of P1F, P2F, P3F, and P4F versus P1L, P2L, P3L, and P4L indicated a wider range of hypo-AF and hypo-IRAF at the posterior fundus, and a partial merging together of the patchy hypo-AF. Choroidal macrovascular morphology was observed in the hypo-IRAF. The junction of hypo-AF and the normal retina and hypo-IRAF and the normal retina of P1 showed the presence of hyper-AF spots and hyper-IRAF spots. The number of hyper-AF spots was significantly greater than the number of hyper-IRAF spots. The position of the hyper-IRAF spots corresponds to the hyper-AF spots, but the hyper-IRAF spots is smaller than hyper-AF spots.

FAF is known to represent mainly fluorescence of lipofuscin [23], while IRAF is mainly melanin fluorescence [24]. Some studies had also observed hyper-AF and hyper-IRAF in AMD. The degradation products of melanin may also be added to lipofuscin with increasing age [25]; therefore, we considered that this phenomenon might also be caused by the accumulation of lipofuscin and melanin degradation products in damaged RPE cells.

The FAF of P2, P3, and P4 showed hyper-AF spots, while the IRAF of P2, P3, and P4 showed choroidal macrovascular morphology in the hypo-IRAF. No hyper-IRAF spots were observed. Considering that the dysfunction of the RPE produced more lipofuscin than melanin degradation products. In P1, hyper-AF spots and hyper-IRAF spots appeared in the hypo-AF and hypo-IRAF peripheral areas. Some hyper-AF spots were observed between the patchy hypo-AF of P2, P3, and P4, which was consistent with the findings of Kojima et al [26], and was considered due to retention of some functions by the impaired RPE.

We had the 4 patients do puzzles for the two FFA examinations to provide a more intuitive and comprehensive view of the progression of the disease. The retinal choroid atrophy was significantly worse in all 8 eyes of the 4 patients in the last than in the first examination, in agreement with previous reports [11, 12]. The left eye and right eye of each patient were essentially the same, but differed among the 4 patients. Normal retinal fluorescence was observed in the mid-peripheral part in P1, and expansion of the lesions was observed from the posterior pole and peripheral parts to the normal retina in the mid-peripheral part. Partial normal retinal fluorescence was observed at the temporal side of the P2 both eyes macular area, and P2L showed a reduction in the area of the normal retina, with expansion of the peripheral lesions to the normal retina. The P3 macular area retina showed no obvious changes, but the surrounding lesions were obviously atrophy aggravations. The P4 both eyes showed less atrophy in the superior temporal area and in the temporal side of the macular area and the inferior peripheral area. The rest of the region was severely atrophied and showed choroidal vascular fluorescence. P4L showed further shrinkage of the less atrophy areas, and the areas with severer atrophy were further extended, with clearer of choroidal macrovascularities. This situation differed from previous research indicating that BCD is an eccentric extension starting from the posterior pole [27, 28, 29, 30]. BCD may not develop exclusively by posterior polar eccentricity as, at least in some cases, the lesion develops from the posterior and peripheral parts and extends to the mid-peripheral part, and the temporal retinal atrophy develops relatively later. This may occur because the temporal retina is farther away from the posterior pole of the BCD initiation site.

In this study, OCT was applied for the first time to quantify the changes in the retina and choroid. The P1 left eye showed increased retinal thickness due to macular edema, an aggravated atrophy of the EZ and RPE, and a thinner choroid. The P1 right eye, P2 both eyes, and P4 both eyes showed thinner retinas, with increased atrophy of the outer retinal nuclear layer, EZ, and RPE and a thinner choroid. The diameter of choroidal macrovascularities was shortened in P1, P2, and P4, consistent with the degenerative properties of the BCD lesions [31]. Our view is that the decrease in the diameter of the choroidal vessels is only one of the reasons for choroidal thinning. We observed that choroidal capillaries also become thinner; however, because the difficulty in defining the boundary of the capillary layer made obtaining specific data impossible. Previous studies have reported reductions in choroidal capillary blood flow, as determined by OCTA [32].

No change, or a change of only a few micrometers, was observed in the P3 macular area measurements, except that the retinal thickness of the right eye fovea thinned to 17 μm, which we did not consider statistically significant. The combination of FAF and FFA results indicated a progression in the retinal choroidal lesions other than in the macular area, but no significant FAF and FFA changes were noted in the macular area. The reflection of the EZ in the P3 macular area was missing. Determining whether this is related to the P3 gene phenotype will require further study on more cases. It was not reported in previous cases [11, 12].

The ORT was first reported in 2009 [33], and it appears in OCT as a low-reflective oval space with a highly reflective boundary in the outer nuclear layer. Since the first report, ORTs have been associated with poor visual prognosis [34, 35, 36]. In our study, ORTs were observed in the two examinations of all 8 eyes, confirming their high incidence in BCD and in agreement with previous results [26, 37]. Two patients in our case showed intraretinal cystoid cavities in the inner nuclear layer in the macular area, suggesting that macular edema is common in BCD. The macular edema in P1 and P4 starts from a zero baseline and progresses from less to more, with adverse effects on the patients' visual acuity. Many previous reports have documented BCD macular cystoid edema [6, 8, 31, 38, 39], but the pathogenesis of the macular cystoid edema is still unclear. The consensus is that it may be the same as the pathogenesis of cystic macular disease in retinal dystrophy, which is caused mainly by damage to the blood-retinal barrier [8, 37, 38]. The exact pathogenesis needs further study.

This study had several limitations, including the small number of included eyes and the lack of primary patient observation. However, considering the rarity of the disease and reviewing the previous literature, our study on the progression of BCD using multimodal images provides one of the largest numbers of images and the largest number of patients. Another limitation is that the large retinal vessels of the P2L right eye and the P4F left eye showed only slight fluorescence in the FAF due to the intravenous injection of the fluorescein sodium test fluid, and this had an impact on the accuracy of our FAF inspections. A third limitation is that the FFA evaluation was not well planned, so the puzzles were inconsistent and some fundus area pictures were missing. A fourth limitation was that the first examination of the 4 patients was retrospective. Therefore, the horizontal B-scan OCT of the P1F left eye and P2F left eye did

not cross the fovea, but slightly deviated from the fovea. Consequently, in the last examination, we used this slightly off-fovea layer for comparison.

Conclusions

Color fundus photography, FAF, IRAF, FFA, and SD-OCT observations of patients with BCD revealed a significant progression in the depth and width of the lesions in a short period of time. FAF, IRAF, and OCT-EDI are all non-invasive examination models, so they have great advantages in detecting disease development and in assessing disease progression. In 2013, Lockhart et al. successfully created a mouse model of BCD [40] and found that retinal crystal deposition and metabolic lipid disorders in the mouse model were very consistent with human BCD. In 2020, Qu et al. used an adeno-associated virus vector to deliver the human CYP4V2 gene to the BCD mouse model through the subretina and showed that the retinal thickness and electroretinogram waveform were effectively restored [41]. The clinical use of gene therapy is therefore anticipated in the near future. Our hope is that the findings presented here can aid in judging the severity of BCD and in treatment selection.

Abbreviations

BCD: Bietti crystalline dystrophy; FAF:Fundus autofluorescence; IRAF:Infrared autofluorescence; FFA:Fundus fluorescein angiography; SD-OCT:Spectral domain optical coherence tomography; ICGA:Indocyanine green angiography; OCT:Optical coherence tomography; EZ:Ellipsoid zone;RPE:Retinal pigment epithelium; BCVA:Best-corrected visual acuity; ETDRS:ETDRS logMAR visual acuity chart; EDI:Enhances the depth imaging; CMT:Central macular thickness; SCT:Subfoveal choroidal thickness; ORT:Outer retinal tubulation; OCTA:Optical coherence tomography angiography

Declarations

Acknowledgments

Not applicable.

Authors' contributions

SJZ and LFW performed the initial clinical database search, identified confirmed cases of BCD, collected all images as presented. SJZ produced the first draft of the manuscript and figures. XYP, QL, LFW and SJZ contributed to the study concept and design, reviewed all the images and statistical analysis and edited the manuscript, contributing to the final version sent for approval.

Funding

The authors did not receive any grant or funds in support of this study

Availability of data and material

The datasets used and/or analysed during the current study are available from the corresponding author on reasonable request.

Ethics approval and consent to participate

This study was approved by the Ethics Committee of Beijing Tongren Hospital, Capital Medical University, and the Ethics Committee of Hebei Provincial Eye Hospital, and was performed in adherence to the principles of the Declaration of Helsinki. Written informed consent was obtained from all participants

Consent for publication

Written informed consent was obtained from the patients for publication of the clinical details and clinical images used in this work.

Competing interests

The authors declare that they have no competing interests.

Author details

[1]Beijing Institute of Ophthalmology, Beijing Ophthalmolgy and Visual Science Key Laboratory, Beijing Tongren Eye Center, Beijing Tongren Hospital, Capital Medical University, 17 Hougou Lane, Chongnei Street, Beijing 100005, People's Republic of China. [2]Hebei Provincial Key Laboratory of Ophthalmology, Hebei Provincial Eye Institute, Hebei Provincial Eye Hospital, 399 East Quanbei Street, Xingtai, Hebei 054001, People's Republic of China.

References

1. Bietti G. B. Uber familiares vorkommen von "Retinitis punctata albescens" (verbunden mit "Dystrophia marginalis cristallinea corneae"), Glitzern des Glasköpers und anderen degenerativen Augenveranderungen. Klinische Monatsblätter für Augenheilkunde. 1937;99:737-56.
2. Lin H, Nishiguchi KM, Nakamura M, Dryja T, Berson E, Miyake Y. Recessive mutations in the CYP4V2 gene in East Asian and Middle Eastern patients with Bietti crystalline corneoretinal dystrophy. J Med Genet. 2005;42(6):e38.
3. Hu DN. Prevalence and mode of inheritance of major genetic eye diseases in China. J Med Genet. 1987;24(10):584-8.
4. Miyata M, Hata M, Ooto S, Ogino K, Gotoh N, Morooka S, et al. Choroidal and retinal atrophy of Bietti crystalline dystrophy patients with CYP4V2 mutations compared to retinitis pigmentosa patients with EYS mutations. Retina. 2017;37:1193-202.
5. Ng DS, Lai TY, Ng TK, Pang CP. Genetics of Bietti crystalline dystrophy. Asia Pac J Ophthalmol. 2016;5(4):245-52.

6. Yin H, Jin C, Fang X, Miao Q, Zhao Y, Chen Z, et al. Molecular analysis and phenotypic study in 14 Chinese families with Bietti crystalline dystrophy. PLoS One. 2014;9(4):e94960.
7. Oishi A, Oishi M, Miyata M, Hirashima T, Hasegawa T, Numa S, et al. Multimodal imaging for differential diagnosis of Bietti crystalline dystrophy. Ophthalmol Retina. 2018;2(10):1071-7.
8. Li Q, Li Y, Zhang X, Xu Z, Zhu X, Ma K, et al. Utilization of fundus autofluorescence, spectral domain optical coherence tomography, and enhanced depth imaging in the characterization of Bietti crystalline dystrophy in different stages. Retina. 2015;35(10):2074-84.
9. Demir ST, Yesiltas SK, Kacar H, Akbas EB, Guven D. Optical coherence tomography and optical coherence tomography angiography imaging in Bietti crystalline dystrophy. Ophthalmic Genet. 2020;41(2):194-7.
10. Nourinia R, Dehghan MH, Fekri S. Outcome of macular hole surgery in Bietti crystalline dystrophy. J Ophthalmic Vis Res. 2017;12(3):338-41.
11. Ipek SC, Ayhan Z, Kadayifcilar S, Saatci AO. Swept-source optical coherence tomography angiography in a patient with Bietti crystalline dystrophy followed for ten years. Turk J Ophthalmol. 2019;49(2):106-8.
12. Mansour AM, Uwaydat SH, Chan CC. Long-term follow-up in Bietti crystalline dystrophy. Eur J Ophthalmol. 2007;17(4):680-2.
13. Yuzawa M, Mae Y, Matsui M. Bietti's crystalline retinopathy. Ophthalmic Paediatr Genet. 1986;7(1):9-20.
14. Margolis R, Spaide RF. A pilot study of enhanced depth imaging optical coherence tomography of the choroid in normal eyes. Am J Ophthalmol. 2009;147:811-5.
15. Kaiser-Kupfer MI, Chan CC, Markello TC, Crawford MA, Caruso RC, Csaky KG, et al. Clinical biochemical and pathologic correlations in Bietti’s crystalline dystrophy. Am J Ophthalmol. 1994;18:569-82.
16. Li A, Jiao X, Munier FL, Schorderet DF, Yao W, Iwata F, et al. Bietti crystalline corneoretinal dystrophy is caused by mutations in the novel gene CYP4V2. Am J Hum Genet. 2004;74:817-26.
17. Haddad NMN, Waked N, Bejjani R, Khoueir Z, Chouery E, Corbani S, et al. Clinical and molecular findings in three Lebanese families with Bietti crystalline dystrophy: report on a novel mutation. Mol Vis 2012;18:1182-8.
18. Yin X, Yang L, Chen N, Cui H, Zhao L, Feng L, et al. Identification of CYP4V2 mutation in 36 Chinese families with Bietti crystalline corneoretinal dystrophy. Exp Eye Res. 2016;46:54-62.
19. Bernauer W, Daicker B. Bietti's corneal-retinal dystrophy. A 16-year progression. Retina. 1992;2(1):18-20.
20. Saatci AO, Yaman A, Oner FH, Ergin MH, Cingil G. Indocyanine green angiography in Bietti's crystalline retinopathy. Can J Ophthalmol. 2002;37(6):346-51.
21. Lee J, Jiao X, Hejtmancik JF, Kaiser-Kupfer M, Gahl WA, Markello TC, et al. The metabolism of fatty acids in human Bietti crystalline dystrophy. Invest Ophthalmol Vis Sci. 2001;42(8):1707-14.

22. Lai TY, Chu KO, Chan KP, Ng TK, Yam GHF, Lam DSC, et al. Alterations in serum fatty acid concentrations and desaturase activities in Bietti crystalline dystrophy unaffected by CYP4V2 genotypes. Invest Ophthalmol Vis Sci. 2010;51(2):1092-7.
23. Sparrow JR, Duncker T. Fundus autofluorescence and RPE lipofuscin in age-related macular degeneration. J Clin Med. 2014;3(4):1302-21.
24. Keilhauer CN, Delori FC. Near-infrared autofluorescence imaging of the fundus: visualization of ocular melanin. Invest Ophthalmol Vis Sci. 2006;47(8):3556-64.
25. Taubitz T, Fang Y, Biesemeier A, Julien-Schraermeyer S, Schraermeyer U. Age, lipofuscin and melanin oxidation affect fundus near-infrared autofluorescence. EbioMedicine. 2019;48:592-604.
26. Kojima H, Otani A, Ogino K, Nakagawa S, Makiyama Y, Kurimoto M, et al. Outer retinal circular structures in patients with Bietti crystalline retinopathy. Br J Ophthalmol. 2012;96:390-3.
27. Mataftsi A, Zografos L, Millá E, Secretan M, Munier F. Bietti's crystalline corneoretinal dystrophy: a cross-sectional study. Retina 2004;24:416-26.
28. Ayata A, Tatlipinar S, Unal M, Ersanli D, Bilge AH. Autofluorescence and OCT features of Bietti's crystalline dystrophy. Br J Ophthalmol. 2008;92:718-20.
29. Liu DN, Liu Y, Meng XH, Yin ZQ. The characterization of functional disturbances in Chinese patients with Bietti's crystalline dystrophy at different fundus stages. Graefes Arch Clin Exp Ophthalmol. 2012;250:191-200.
30. Toto L, Carpineto P, Parodi MB, Di Antonio L, Mastropasqua A, Mastropasqua L. Spectral domain optical coherence tomography and in vivo confocal microscopy imaging of a case of Bietti's crystalline dystrophy. Clin Exp Optom. 2013;96:39-45.
31. Saatci AO, Doruk HC, Yaman A, Oner FH. Spectral domain optical coherence tomographic findings of bietti crystalline dystrophy. J Ophthalmol. 2014;2014:739271.
32. Miyata M, Oishi A, Hasegawa T, Ishihara K, Oishi M, Ogino K, et al. Choriocapillaris flow deficit in Bietti crystalline dystrophy detected using optical coherence tomography angiography. Br J Ophthalmol. 2018;102:1208-12.
33. Zweifel SA, Engelbert M, Laud K, Margolis R, Spaide RF, Freund KB. Outer retinal tubulation: a novel optical coherence tomography finding. Arch Ophthalmol. 2009;127(12):1596-602.
34. Faria-Correia F, Barros-Pereira R, Queiros-Mendanha L, Fonseca S, Mendonca L, Falcao MS, et al. Characterization of neovascular age-related macular degeneration patients with outer retinal tubulations. Ophthalmologica. 2013;229(3):147-51.
35. Lee JY, Folgar FA, Maguire MG, Ying GS, Toth C, Martin DF, et al. Outer retinal tubulation in the comparison of age-related macular degeneration treatments trials (CATT). Ophthalmology. 2014;121(12):2423–31.
36. Dolz-Marco R, Litts KM, Tan ACS, Freund KB, Curcio CA. The evolution of outer retinal tubulation, a neurodegeneration and gliosis prominent in macular diseases. Ophthalmology. 2017;124(9):1353-67.

37. Goldberg NR, Greenberg JP, Laud K, Tsang S, Freund KB. Outer retinal tubulation in degenerative retinal disorders. Retina. 2013;33:1871-6.
38. Broadhead GK, Chang AA. Acetazolamide for cystoid macular oedema in Bietti crystalline retinal dystrophy. Korean J Ophthalmol. 2014;28:189-91.
39. Salvatore S, Fishman GA, Genead MA. Treatment of cystic macular lesions in hereditary retinal dystrophies. Surv Ophthalmol. 2013;58:560-84.
40. Lockhart CM, Nakano M, Rettie AE, Kelly EJ. Generation and characterization of a murine model of Bietti crystalline dystrophy. Invest Ophthalmol Vis Sci. 2014;55:5572-81.
41. Qu B, Wu S, Jiao G, Zou X, Li Z, Gou L, et al. Treating Bietti crystalline dystrophy in a high-fat diet-exacerbated murine model using gene therapy. Gene Ther. 2020;27(7-8):370-82.

Tables

Table 1. Clinical Data

Patient	Sex	Age	Stage	Check Interval (months)	Check code	BCVA ETDRS	
						OD	OS
P1	M	38	2	10	P1F	34	80
					P1L	2	77
P2	F	38	2	16	P2F	85	72
					P2L	78	61
P3	M	34	3	20	P3F	66	74
					P3L	46	64
P4	M	29	3	20	P4F	81	69
					P4L	67	50

Check Interval: the interval between two examinations for the same patient (shown as months). BCVA: best corrected visual acuity. ETDRS: ETDRS logMAR visual acuity chart. F, female; M, male; N, none; OD, right eye; OS, left eye.

Table 2. Genetic and Consanguinity Status

Patient	Genetic Analysis		Consanguinity
	Allele 1	Allele 2	
P1	c.802-8_810del17insGC	c.802-8_810del17insGC	N
P2	c.992A>C,p.H331P	c.992A>C,p.H331P	N
P3	c.802-8_810del17insGC	c.332T>C;p.I111T	N
P4	c.802-8_810del17insGC	C.1091-2A>G;g.17344A>G,rs199476183	N

N, no.

Table 3. Comparison of two OCT measurement results (strUnit： μm)

Patient	DBTM	CMT		SCT		DSTCV		DSNCV		LEZ		DBFE	
		OD	OS	OD	OS	OD	OS	OD	OS	OD	OS	OD	OS
P1	P1F-P1L	51	-12	72	88	28	32	38	27	N	169	-165	UM
P2	P2F-P2L	15	73	29	25	20	40	19	17	476	393	N	N
P3	P3F-P3L	17	0	4	9	8	4	0	0	N	N	N	N
P4	P4F-P4L	11	4	94	24	31	6	24	10	72	237	N	N

DBTM: difference between two measurements. CMT: central macular thickness; SCT: subfoveal choroidal thickness;

DSTCV: the diameter of a subfoveal temporal choroidal vessel. DSNCV: the diameter of a subfoveal nasal choroidal vessel. LEZ: the length of the ellipsoid zone (EZ) in the fovea. DBFE: distance between fovea and the remnant of the temporal EZ. UM, unmeasured. N, no. Y, yes.

Figures

Fig.1

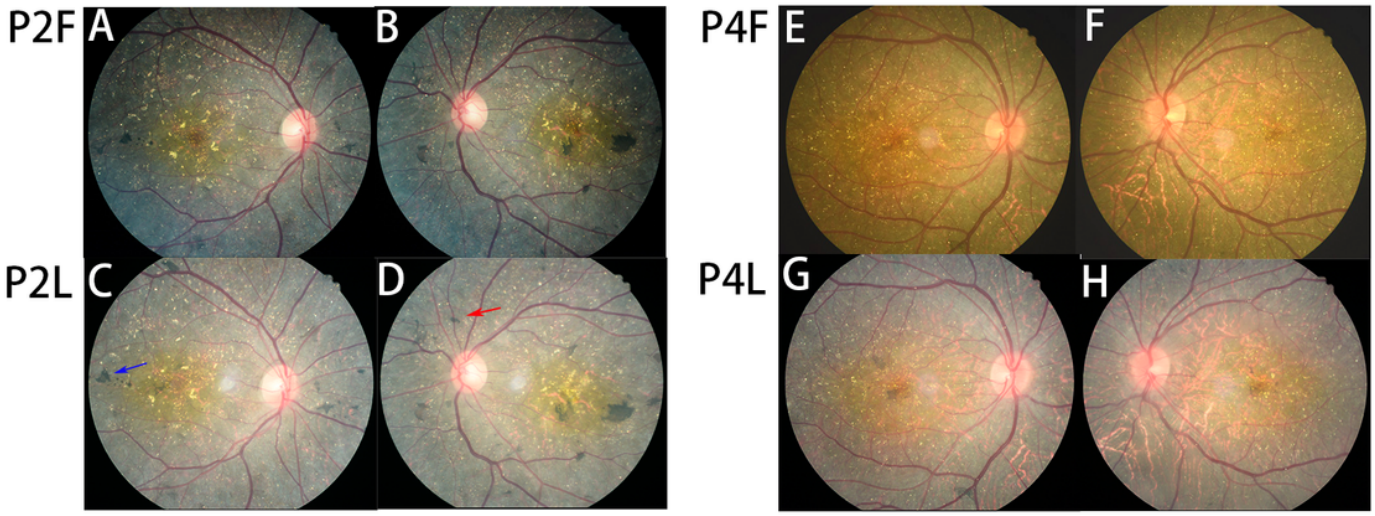

Figure 1

Color fundus photography images of P2 and P4 with BCD. A-D Fundus photographs (color) of P2. E-H Fundus photographs (color) of P4. The yellowish crystalline deposits in the posterior pole of the retina were reduced at the last examination. The increscent pigment plaques (blue arrow) and the newly increased pigment plaques (red arrow) are shown.

Fig.1

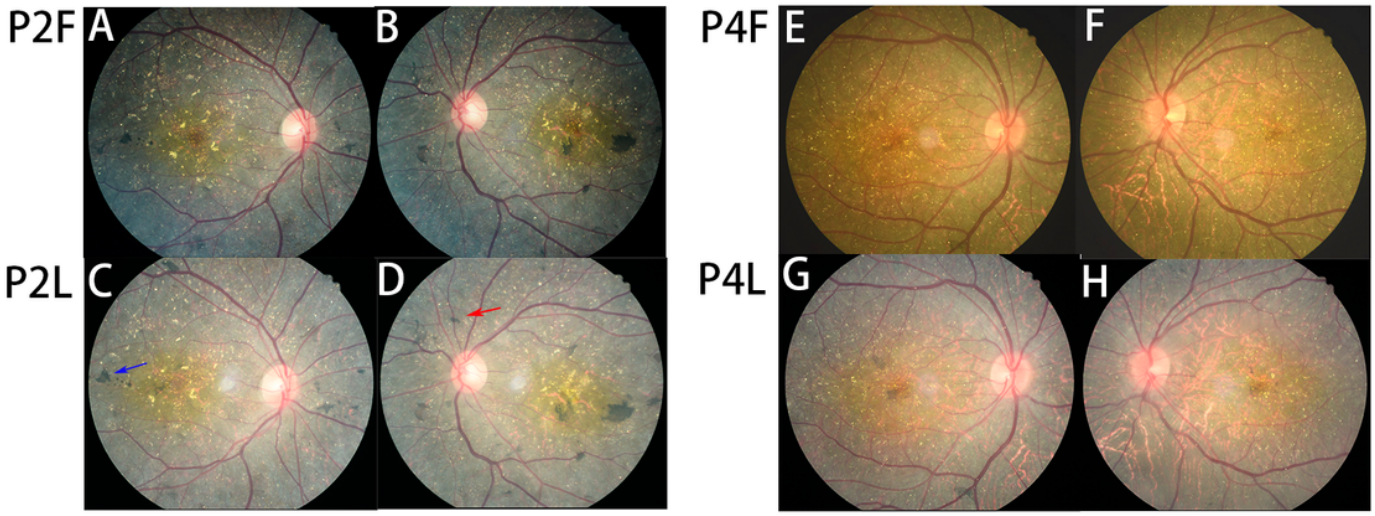

Figure 1

Color fundus photography images of P2 and P4 with BCD. A-D Fundus photographs (color) of P2. E-H Fundus photographs (color) of P4. The yellowish crystalline deposits in the posterior pole of the retina were reduced at the last examination. The increscent pigment plaques (blue arrow) and the newly increased pigment plaques (red arrow) are shown.

Fig.2

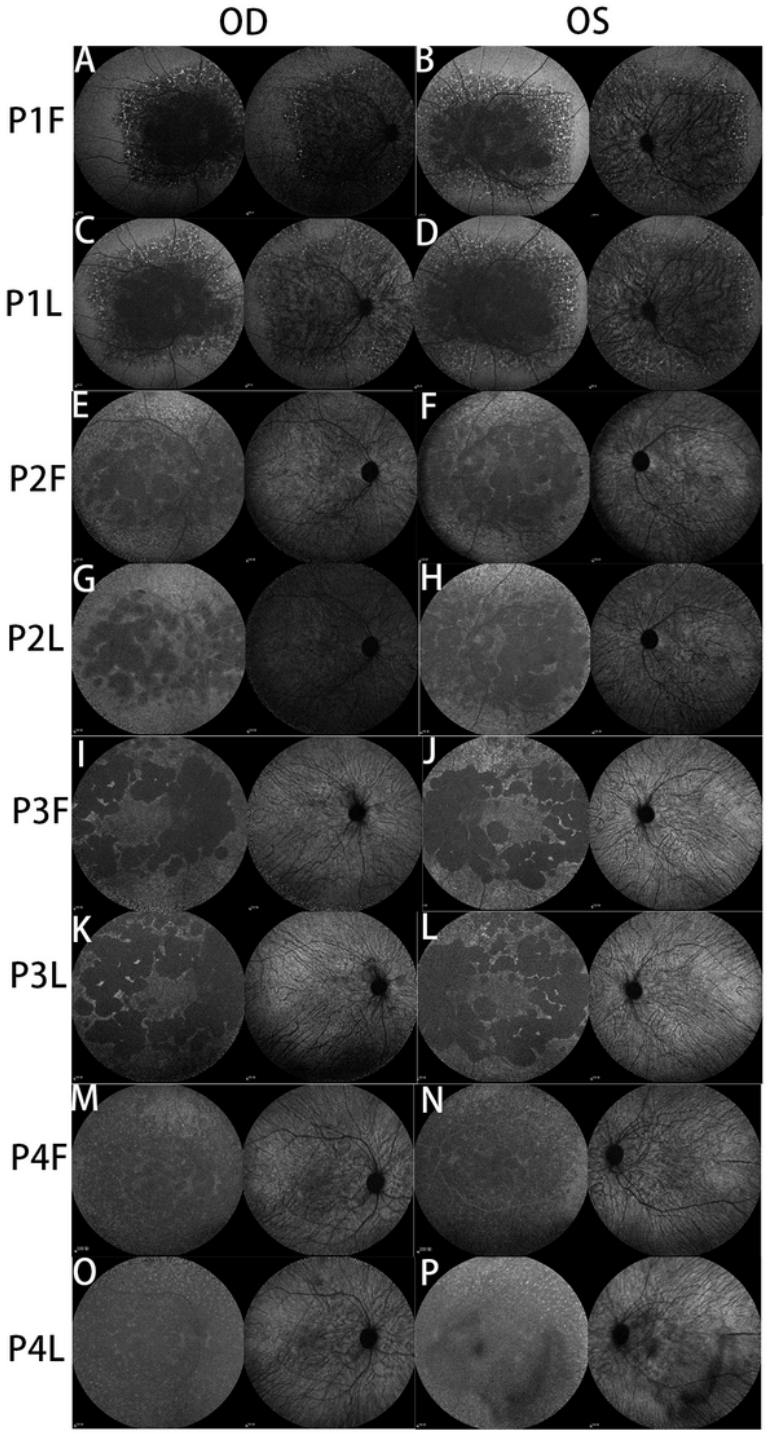

Figure 2

Fundus autofluorescence and infrared autofluorescence images of P1-P4. A-D show similar lesion ranges of FAF and IRAF in the P1 both eyes, and a significant expansion of the lesion range of the P1L both eyes compared to the P1F both eyes. The junction of the lesion and the normal retina shows hyper-AF spots and hyper-IRAF spots, and the number of hyper-AF spots is significantly greater than the number of hyper-IRAF spots. Patchy hypo-AF are partially merged together. IRAF shows the hypo-IRAF choroidal macrovascular morphology in the posterior lesion area. E-H show expansion of the P2 both eyes hypo-AF range, with patchy hypo-AF partially merged together. A small number of hyper-IRAF spots are shown in the P2F both eyes, but no hyper-IRAF spots are shown in the P2L both eyes. I-L show significant expansion of the hypo-AF range of the P3L both eyes compared with the P3F both eyes, patchy hypo-AF partially merged together, and the hyper-AF spots disappeared. IRAF shows the hypo-IRAF morphology of optic disc, retinal macrovascularities, and choroidal macrovascularities, but no hyper-IRAF spots. M-P show significant expansion of the hypo-AF area of P4L both eyes compared with the P4F both eyes. The patchy hypo-AF partially merged together, and hyper-AF spots are shown. IRAF shows the hypo-IRAF of optic disc, retinal macrovascularities, and choroidal macrovascularities, but no hyper-IRAF spots.

Fig.2

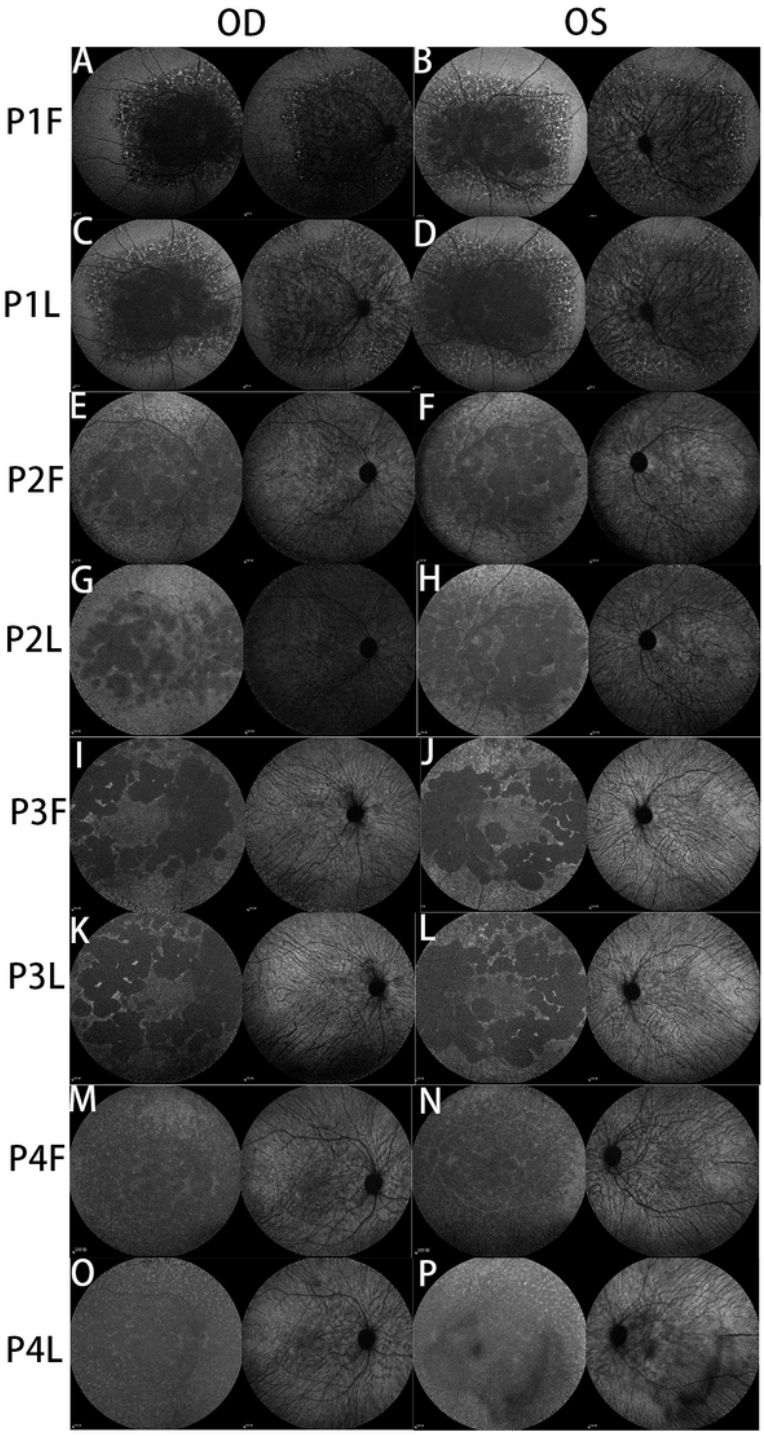

Figure 2

Fundus autofluorescence and infrared autofluorescence images of P1-P4. A-D show similar lesion ranges of FAF and IRAF in the P1 both eyes, and a significant expansion of the lesion range of the P1L both eyes compared to the P1F both eyes. The junction of the lesion and the normal retina shows hyper-AF spots and hyper-IRAF spots, and the number of hyper-AF spots is significantly greater than the number of hyper-IRAF spots. Patchy hypo-AF are partially merged together. IRAF shows the hypo-IRAF choroidal

macrovascular morphology in the posterior lesion area. E-H show expansion of the P2 both eyes hypo-AF range, with patchy hypo-AF partially merged together. A small number of hyper-IRAF spots are shown in the P2F both eyes, but no hyper-IRAF spots are shown in the P2L both eyes. I-L show significant expansion of the hypo-AF range of the P3L both eyes compared with the P3F both eyes, patchy hypo-AF partially merged together, and the hyper-AF spots disappeared. IRAF shows the hypo-IRAF morphology of optic disc, retinal macrovascularities, and choroidal macrovascularities, but no hyper-IRAF spots. M-P show significant expansion of the hypo-AF area of P4L both eyes compared with the P4F both eyes. The patchy hypo-AF partially merged together, and hyper-AF spots are shown. IRAF shows the hypo-IRAF of optic disc, retinal macrovascularities, and choroidal macrovascularities, but no hyper-IRAF spots.

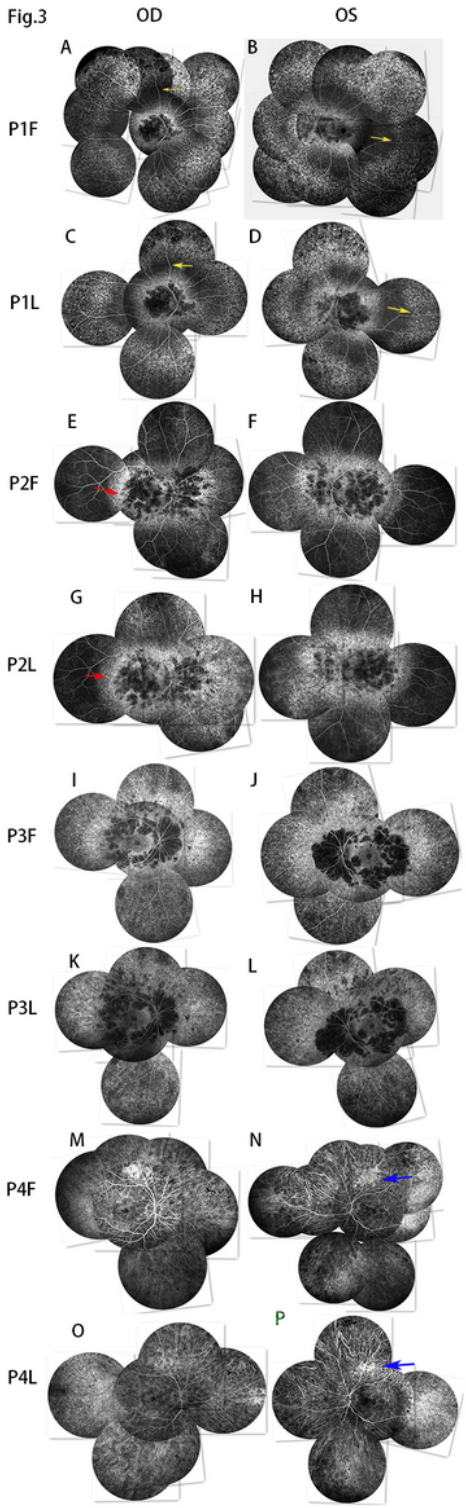

Figure 3

Fundus fluorescein angiography images of P1-P4. A-H show a comparison of P1L versus P1F, and of P2L versus P2F, and demonstrates an expansion of the hypo-fluorescence in the posterior area (red arrows). The mottled fluorescence around the hypo-fluorescence and the mottled fluorescence at the periphery (yellow arrows) all expanded to the middle periphery. I-L show a large hypo-fluorescence area in the posterior and middle peripheral area of the P3 both eyes, while the peripheral area shows mottled

fluorescence. M-P show a slight residual mottled fluorescence area (blue arrows), and the whole fundus show a large area of choroidal macrovascular fluorescence. I-P show P3L versus P3F and P4L versus P4F. The retinal mottled fluorescence area is significantly reduced, and the choroidal macrovascularities are more clearer.

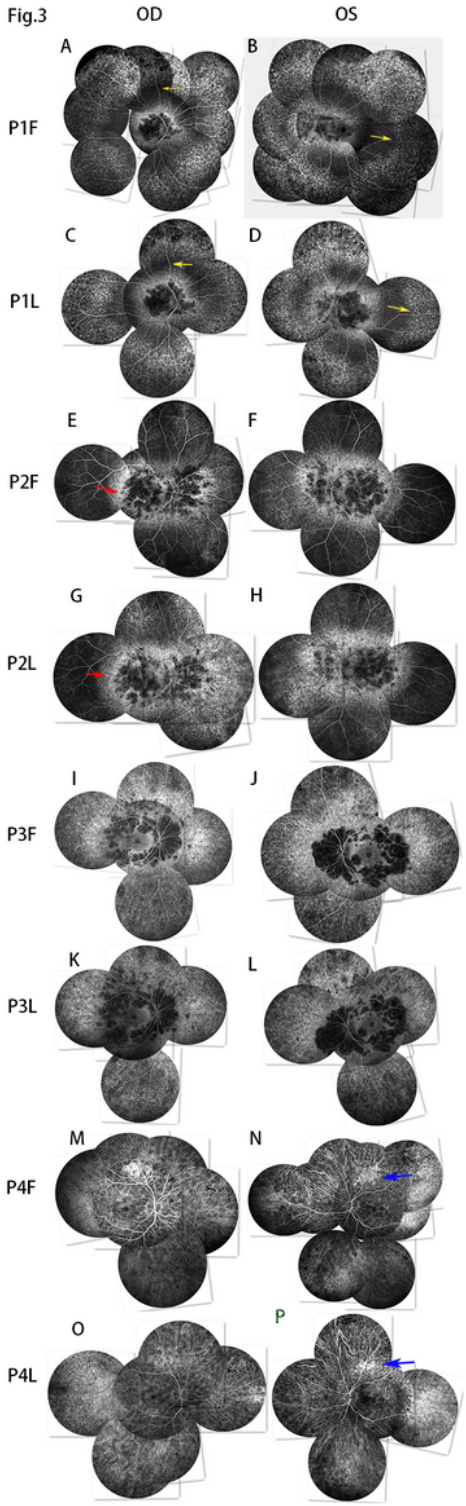

Figure 3

Fundus fluorescein angiography images of P1-P4. A-H show a comparison of P1L versus P1F, and of P2L versus P2F, and demonstrates an expansion of the hypo-fluorescence in the posterior area (red arrows). The mottled fluorescence around the hypo-fluorescence and the mottled fluorescence at the periphery (yellow arrows) all expanded to the middle periphery. I-L show a large hypo-fluorescence area in the posterior and middle peripheral area of the P3 both eyes, while the peripheral area shows mottled fluorescence. M-P show a slight residual mottled fluorescence area (blue arrows), and the whole fundus show a large area of choroidal macrovascular fluorescence. I-P show P3L versus P3F and P4L versus P4F. The retinal mottled fluorescence area is significantly reduced, and the choroidal macrovascularities are more clearer.

Fig.4

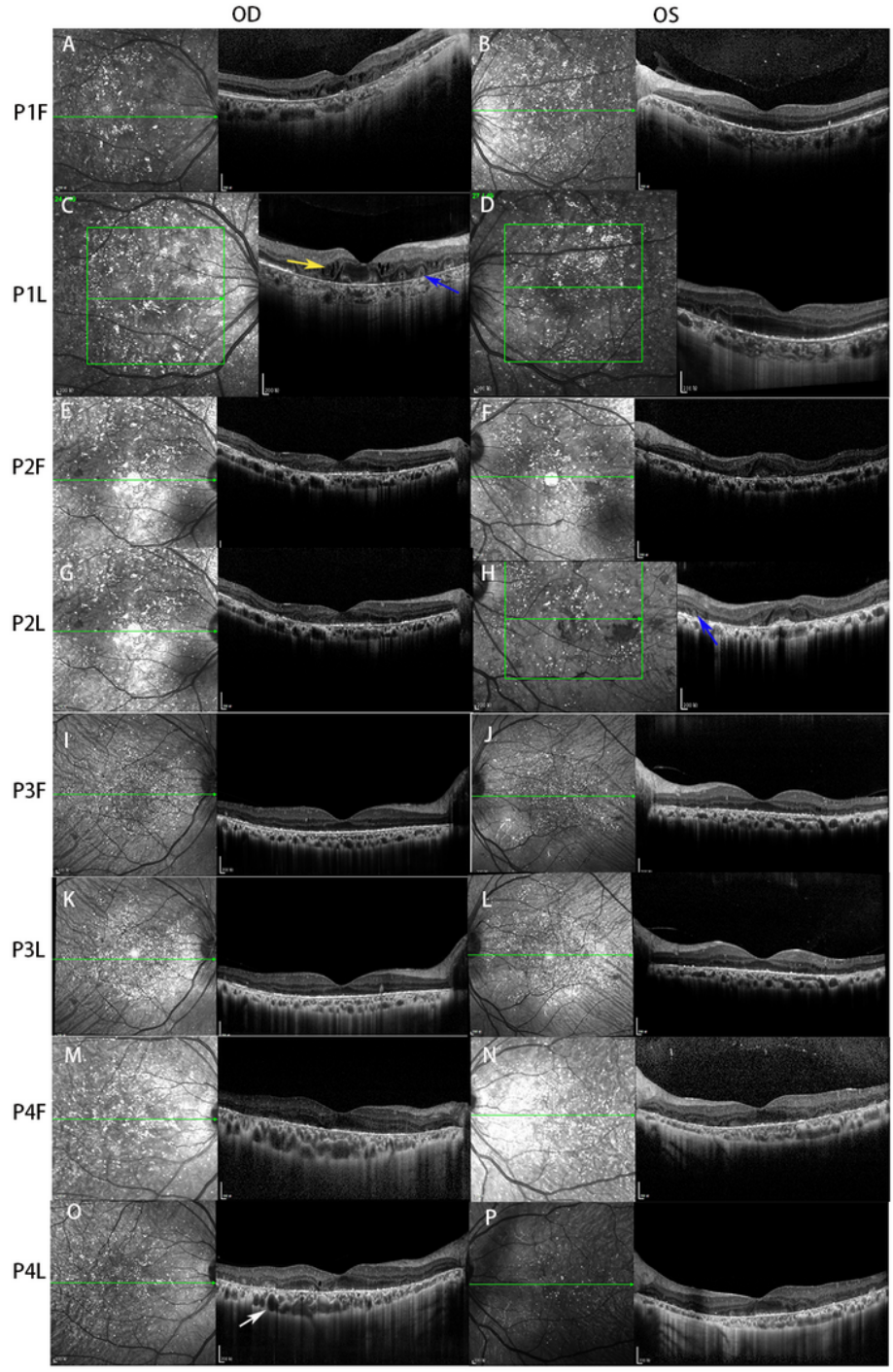

Figure 4

Spectral domain optical coherence tomography images of P1-P4. A-D show greater increases in the edema in the macular fovea of P1L than in P1F. The liquid cystoid cavities were mainly in the inner nuclear layer (yellow arrow), the outer nuclear layer was thickened, and the ellipsoid zone was reduced more in P1L than in P1F. E-H and M-P show P2 and P4 retain the ellipsoid zone at the fovea, and the ellipsoid zones of P2L and P4L are more atrophic than those of P2F and P4F; the choroidal vessels also

become thinner (white arrow). I-L show that the ellipsoid zone and interdigitation zone are missing in the macular area of P3. P3L has no obvious changes compared with P3F. The outer retinal tubulations (ORT) are seen in some layers (blue arrows).

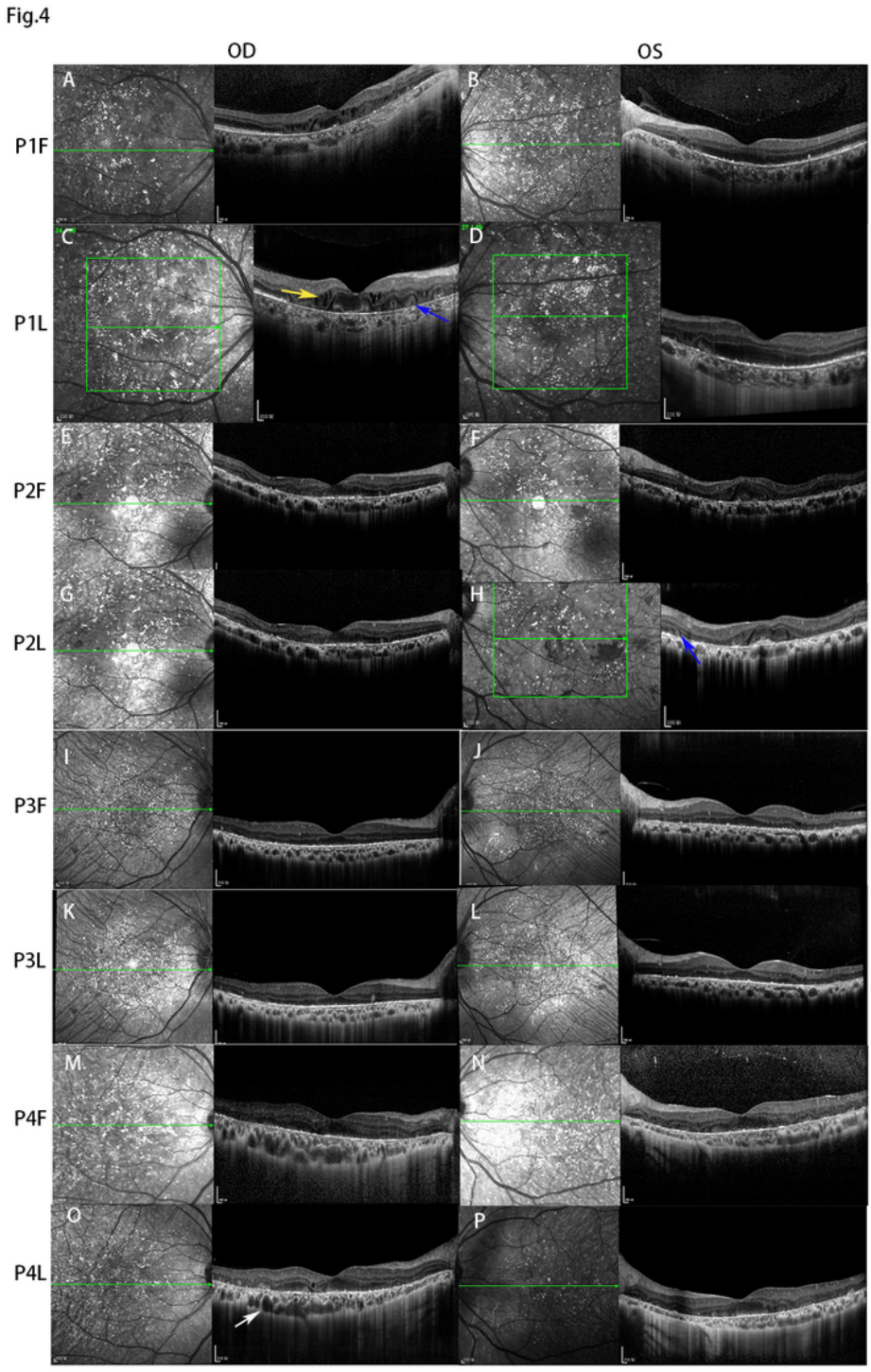

Figure 4

Spectral domain optical coherence tomography images of P1-P4. A-D show greater increases in the edema in the macular fovea of P1L than in P1F. The liquid cystoid cavities were mainly in the inner

nuclear layer (yellow arrow), the outer nuclear layer was thickened, and the ellipsoid zone was reduced more in P1L than in P1F. E-H and M-P show P2 and P4 retain the ellipsoid zone at the fovea, and the ellipsoid zones of P2L and P4L are more atrophic than those of P2F and P4F; the choroidal vessels also become thinner (white arrow). I-L show that the ellipsoid zone and interdigitation zone are missing in the macular area of P3. P3L has no obvious changes compared with P3F. The outer retinal tubulations (ORT) are seen in some layers (blue arrows).